

A hot X-ray filament associated with A3017 galaxy cluster

V. Parekh, F. Durret, P. Padmanabh, M. B. Pandge

▶ **To cite this version:**

V. Parekh, F. Durret, P. Padmanabh, M. B. Pandge. A hot X-ray filament associated with A3017 galaxy cluster. Monthly Notices of the Royal Astronomical Society, 2017, 470, pp.3742-3749. 10.1093/mnras/stx1457 . insu-03747436

HAL Id: insu-03747436

https://insu.hal.science/insu-03747436

Submitted on 8 Aug 2022

HAL is a multi-disciplinary open access archive for the deposit and dissemination of scientific research documents, whether they are published or not. The documents may come from teaching and research institutions in France or abroad, or from public or private research centers.

L'archive ouverte pluridisciplinaire **HAL**, est destinée au dépôt et à la diffusion de documents scientifiques de niveau recherche, publiés ou non, émanant des établissements d'enseignement et de recherche français ou étrangers, des laboratoires publics ou privés.

Monthly Notices
of the
ROYAL ASTRONOMICAL SOCIETY

MNRAS **470,** 3742–3749 (2017)
Advance Access publication 2017 June 13

doi:10.1093/mnras/stx1457

A hot X-ray filament associated with A3017 galaxy cluster

V. Parekh,[1]★ F. Durret,[2] P. Padmanabh[3] and M. B. Pandge[4]†

[1]*Raman Research Institute, C. V. Raman Avenue, Sadashivnagar, Bangalore 560080, India*
[2]*Institut d'Astrophysique de Paris, CNRS, 98bis Bd. Arago, F-75014 Paris, France*
[3]*Inter-University Centre for Astronomy and Astrophysics, Post Bag 4, Ganeshkhind, Pune 411007, India*
[4]*Dayanand Science College, Barshi Road, Latur, Maharashtra 413512, India*

Accepted 2017 June 8. Received 2017 June 7; in original form 2017 March 14

ABSTRACT

Recent simulations and observations have shown large-scale filaments in the cosmic web connecting nodes, with accreting materials (baryonic and dark matter) flowing through them. Current high-sensitivity observations also show that the propagation of shocks through filaments can heat them up and make filaments visible between two or more galaxy clusters or around massive clusters, based on optical and/or X-ray observations. We are reporting here the special case of the cluster A3017 associated with a hot filament. The temperature of the filament is $3.4^{-0.77}_{+1.30}$ keV and its length is ∼1 Mpc. We have analysed its archival *Chandra* data and report various properties. We also analysed GMRT 235/610 MHz radio data. Radio observations have revealed symmetric two-sided lobes that fill cavities in the A3017 cluster core region, associated with central active galactic nucleus. In the radio map, we also noticed a peculiar linear vertical radio structure in the X-ray filament region which might be associated with a cosmic filament shock. This radio structure could be a radio phoenix or old plasma where an old relativistic population is re-accelerated by shock propagation. Finally, we put an upper limit on the radio luminosity of the filament region.

Key words: radio continuum: general – X-rays: galaxies: clusters.

1 INTRODUCTION

Recent cosmological *N*-body simulations show that strong concentrations of matter appear to be interlinked by large, low-density filaments (Springel et al. 2005; Dolag, Bykov & Diaferio 2008), surrounded by almost empty voids. This overall pattern is commonly known as the 'Cosmic Web'. According to the Λ cold dark matter model the highest mass concentrations reside at the intersection points of dark matter filaments, through which they accrete both dark and baryonic mass and grow over time. These interconnecting filaments have too low a density contrast to be easily detectable by weak lensing (Dietrich et al. 2012). However, when two extremely large mass concentrations, such as two galaxy clusters, come relatively close to each other (∼ order of Mpc distance), the mass density of the filament/bridge between them is expected to be higher than the mean and might be detectable. Hence, binary galaxy clusters are the ideal locations to search for large-scale matter filaments and understand their role in structure formation. Furthermore, galaxy clusters grow in mass due to (i) merging with other cluster(s) and (ii) accretion of matter. The first process leads to the X-ray substructures due to heating and mixing of intracluster gas, and the later process proceeds via supersonic inflows near the virial radii of clusters. This accretion process happens predominantly through the filaments that are connected to the clusters in their outskirts. The study of filaments is extremely important to understand cluster growth processes at the filamentary nodes and the acceleration of high energy particles via shocks and turbulence.

Current and future X-ray observations will allow us to select galaxy cluster targets to study filaments. High-quality *Chandra* and *XMM–Newton* X-ray observations have already detected filaments during these last years (Durret et al. 2003; Werner et al. 2008; Planck Collaboration VIII 2013). Recently, Eckert et al. (2015) have detected filamentary structures associated with the A2744 galaxy cluster with the *Chandra* X-ray telescope. These filaments are in agreement with the positions of overdensities of cluster galaxies and dark matter. This result supports evidence for the hypothesis in which a large fraction of the missing baryons of the Universe reside in the filaments of the cosmic web. Previously, Kull & Böhringer (1999) have detected filamentary X-ray structure in the core region of the Shapley supercluster (between A3556 and A3558), Werner et al. (2008) have detected hot gas in the filament connecting the clusters of galaxies A222 and A223, and Buote et al. (2009) have also reported filaments between A2804 and A2811 in the Sculptor supercluster based on X-ray absorption lines.

X-ray observations with subarcsecond resolution also revealed a variety of substructures – cavities, bubbles, spiral features, cold

★ E-mail: viral.iucaa@gmail.com
† DST INSPIRE Faculty.

© 2017 The Authors
Published by Oxford University Press on behalf of the Royal Astronomical Society

Downloaded from https://academic.oup.com/mnras/article/470/3/3742/3867312 by CNRS - ISTO user on 08 August 2022

Table 1. A3017 properties.

Cluster name	RA(J2000) (h m s)	Dec.(J2000) (d m s)	z	Luminosity [10^{44} erg s^{-1} (0.1–2.4 keV)]	$Y_X\ M_{500}$ (10^{14} M$_\odot$)
A3017	02 25 52	−41 54.5	0.2195	10.17	5.81

fronts, etc. – in the core of galaxy clusters (Vikhlinin & Markevitch 2002; Markevitch & Vikhlinin 2007; McNamara & Nulsen 2007; Blanton et al. 2011; McNamara & Nulsen 2012; Paterno-Mahler et al. 2013). The central active galactic nucleus (AGN) plays an active role in creating cavities and bubbles. In an investigation of a large sample of such systems, it was revealed that a central radio source was present in every system, with the radio plasma (or radio lobes) often filling the cavities and bubbles. The X-ray cavities and bubbles are therefore interpreted as regions where the X-ray emitting gas has been displaced by radio plasma produced by energetic outflows from the AGN that injects significant power into the ICM. Hence, the central AGN is thought to be a heating source providing feedback to compensate for the excessive cooling of the cluster core.

Spiral features are likely related to 'sloshing' of the ICM in the core of the cluster (Blanton et al. 2011). Simulations (Ascasibar & Markevitch 2006; ZuHone, Markevitch & Lee 2011) have shown that the off-centre collision of a cluster with a galaxy group, with mass ratios between 1/2 and 1/10, accelerates both the dark matter component and the cool gas of the cluster core, but the gas component is decelerated by ram pressure, resulting in a separation between the dark matter and the baryons. As the ram pressure weakens, the cool core gas falls back into the potential well, but overshoots it and begins to 'slosh'. Heating of the ICM may also result from gas 'sloshing' in the cluster central potential well. However, it has been noticed that this mechanism is efficient to move the cool gas from the centre but it cannot stop or regulate the cluster cooling flow.

A3017 ($z = 0.2195$) is a peculiar cluster system that we discovered to be clearly displaying the extremely rare occurrence of a large-scale ($\sim$ Mpc) intercluster matter filament. The hot, gaseous filament extending on the Mpc scale was discovered in *Chandra* X-ray observations (above 5σ detection). This filament is much hotter and more X-ray luminous than the filamentary bridge between the A222/A223 cluster pair (Werner et al. 2008). In addition to this, a pair of AGN-related X-ray cavities at the core region of A3017, one infalling group and several other groups interacting within A3017 are also detected. All these features make A3017 a prime target for studies. We also obtained its 235/610 MHz dual frequency GMRT data. We have listed the properties of A3017 in Table 1. We assume $H_0 = 70$ km s^{-1} Mpc^{-1}, $\Omega_M = 0.3$ and $\Omega_\Lambda = 0.7$ throughout the paper. At a redshift of 0.2195, the physical size of 1 arcsec is 3.55 kpc.

2 X-RAY AND RADIO OBSERVATIONS

2.1 X-ray data analysis

We used *Chandra* archival data to study A3017 (Table 2). We followed standard X-ray data analysis and processed the data with CIAO 4.8 and CALDB 4.7.0. We first used the `chandra_repro` task to reprocess all ACIS imaging data, removed high background flares (3σ clipping) with the task `lc_sigma_clip` and combined multiple data sets with the `merge_obs` script. All event files included the 0.3–7 keV broad energy band and 2 arcsec pixel binning. We removed point sources around the cluster and filament region. We divided the count image by the exposure map and generated the flux image (photon cm^{-2} s^{-1}). For the spectral analysis work, we used the CIAO SHERPA V1 package. For background estimation, we used *Chandra* blank sky files.

Table 2. A3017 *Chandra* X-ray data.

Obsid	Instrument	Obsdate	Exposure time (ks)
15110	ACIS-I	2013-05-01	14.8
17476	ACIS-I	2015-04-21	13.8

2.2 Radio data analysis

We observed the A3017 cluster in the dual frequency 610/235 MHz band with GMRT in 2015 August for a total duration of $\sim$6 h (PI: V. Parekh, obsid. 28_087). This allows to record one polarization in each frequency band (610 MHz with RR and 235 MHz with LL). The GMRT software back-end with a bandwidth of 12 and 32 MHz at 235 and 610 MHz frequencies, respectively, were used in these observations. The data were processed with a fully automated pipeline based on the SPAM package (Intema et al. 2009; Intema 2014), which includes direction-dependent calibration, modelling and imaging to suppress mainly ionospheric phase errors. In summary, the pipeline consists of two parts: a *pre-processing* part that converts the raw data from individual observing sessions into pre-calibrated visibility data sets for all observed pointings and a *main pipeline* part that converts pre-calibrated visibility data per pointing into stokes I continuum images. The flux scale is set by calibration on 3C48 using the models from Scaife & Heald (2012). We used default robust -1 weighting value in the SPAM to make images. More details on the processing pipeline and characteristics of the data products are given in paper on the first TGSS alternative data release (ADR1; Intema et al. 2017).

2.3 Images

As shown in Fig. 1(a), there is a filament of $\sim$1 Mpc projected size visible in X-rays, which seems to connect the A3017 (north) and south X-ray clusters. The core-to-core (X-ray peak-to-peak) distance between them is $\sim$470 arcsec, corresponding to a physical size of $\sim$1.7 Mpc. There is an Abell cluster, A3016, situated at RA: $02^h25^m22\overset{s}{.}1$ and Dec.: $-42^\circ00'30''$. However, it is unclear that the south X-ray cluster is associated with A3016 or not. There is an offset of $\sim$45 arcsec ($\sim$160 kpc at the cluster redshift) between the X-ray peak of the south cluster and the position of A3016. See Section 4 for the redshift analysis of A3016.

We used double 2D beta models to subtract the surface brightness model from the cluster X-ray image. Its residual shows several interesting features. In addition to the filament between clusters, there are two symmetric cavities present in the core of A3017 (Fig. 1b). Further there are two X-ray peaks lying in the north–south direction in the core of the cluster: a northern peak associated with radio and optical counterparts which could be a BCG and a southern peak

Downloaded from https://academic.oup.com/mnras/article/470/3/3742/3867312 by CNRS - ISTO user on 08 August 2022

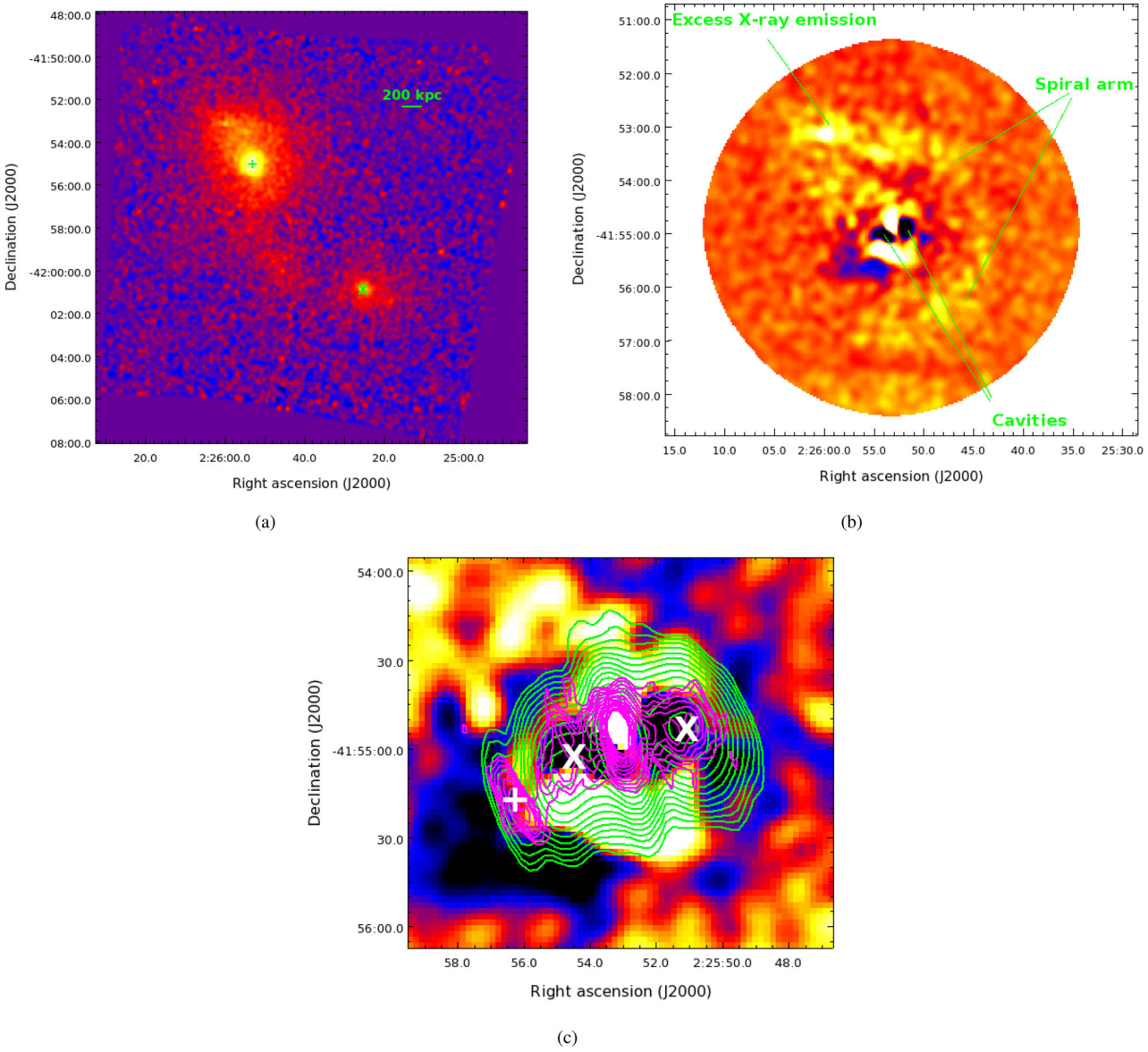


Figure 1. (a) Background-subtracted and exposure-corrected *Chandra* ACIS-I X-ray image. A3017 is marked with a '+' and the south X-ray cluster with an '×' sign. (b) Central core region of A3017. (c) Zoom of the A3017 core region with radio contours (green for 235 MHz and magenta for 610 MHz GMRT data). In this image, we marked the lobes ('×') and unresolved radio source ('+'). The first radio contour is drawn at 5σ and the levels increase in steps of $\sqrt{2}$. At 235 MHz, 1σ rms is ∼0.45 mJy/beam; and at 610 MHz, 1σ rms is ∼60 μJy/beam. Both radio images are shown with their original resolutions. Resolution of the 235 MHz image is 25 arcsec × 9 arcsec, pa = 14.°5 and of the 610 MHz image is 10 arcsec × 4 arcsec, pa = 14°.

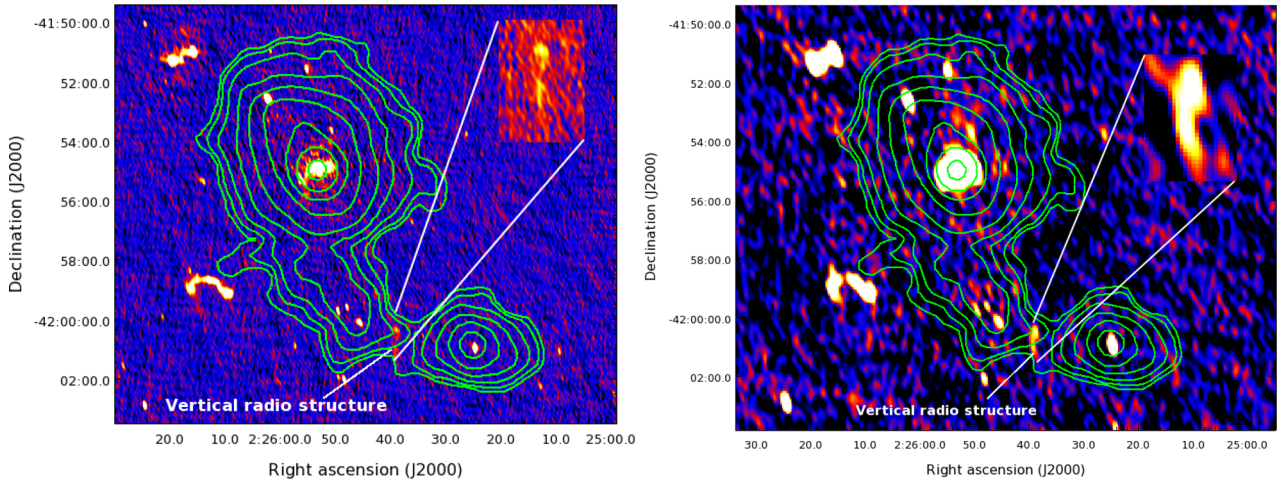
associated with X-ray emission. The distance between these two peaks is ∼12 arcsec. Two X-ray cavities situated around the two peaks within ∼20 arcsec from the BCG may indicate a young AGN from which the jet and lobe expansion has just started. These cavities are very likely large empty bubbles evacuated by the AGN radio lobes. In radio 235 and 610 MHz GMRT data (Fig. 1c), we can see two radio lobes around the BCG and they fill the opposite X-ray cavities (marked with '×'). We noticed that the east and west lobes have similar sizes, but the west lobe is more powerful than the east lobe. We also marked an unresolved radio source (left to the east lobe) in this radio image, with '+'. In Table 3, we listed the radio properties of the lobes and the central radio source. We found steep spectra for the lobes and the central radio source, with spectral indices of ∼−2.6, ∼−3.3 and ∼−1.3 for the west lobe, the east lobe and the central radio source, respectively.

Table 3. A3017 radio lobes and BCG properties.

Frequency (MHz)	Region	Size (″ × ″)	Flux density (mJy)	Radio power (W Hz^{-1})
235	West lobe	20 × 10	303 ± 30	25.63
–	East lobe	24 × 9	250 ± 25	25.55
–	BCG	9 × 5	514 ± 51	–
610	West lobe	26 × 16	25 ± 2.5	24.55
–	East lobe	19 × 13	10 ± 1.0	24.15
–	BCG	7 × 5	138 ± 13	–

In this residual image, as shown in Fig. 1(b), there is an excess X-ray emission visible in the north-east direction of A3017. It could be associated with infalling groups of galaxies, as suggested in the case of Abell 85 (Durret, Lima Neto & Forman 2005). This excess

Downloaded from https://academic.oup.com/mnras/article/470/3/3742/3867312 by CNRS - ISTO user on 08 August 2022



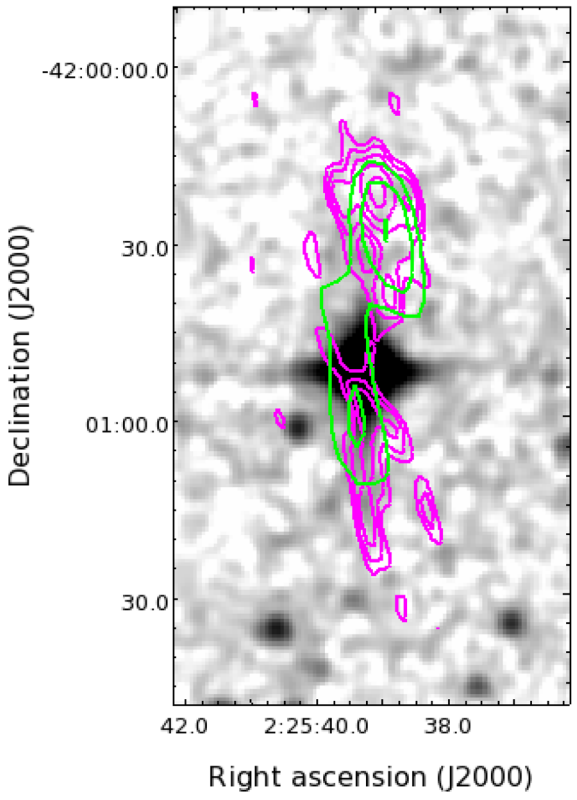


Figure 2. (a) High resolution 610 MHz radio image (colour) and *Chandra* X-ray contours (green). (b) High resolution 235 MHz radio image (colour) and *Chandra* X-ray contours (green). In both images the peculiar vertical radio structure on the X-ray bridge region is highlighted within the inset. (c) Contours of the vertical radio structure at 235 (green) and 610 MHz (magenta) superimposed on the optical SuperCOSMOS image. There is no optical counterpart associated with this structure. The first radio contour is drawn at 3σ and the levels increase in steps of $\sqrt{2}$. The rms noise values are the same as mentioned in the caption to Fig. 1.

X-ray emission connects with the cluster core region in the east-south direction and towards the west connects with the large spiral arm extending towards the south around the cluster core. The radius of this spiral arm is ∼110 arcsec. This spiral arm could be connected with the intercluster filament at the cluster outskirts. Moreover, we also noticed a very peculiar, narrow and extended radio structure in the filamentary X-ray bridge region in both 610 and 235 MHz radio images, as shown in the zoom in the image subset of Fig. 2. The angular (linear) size of this radio structure, placed perpendicular to the filament axis, is ∼85 arcsec (300 kpc) and ∼65 arcsec (230 kpc) at 610 and 235 MHz, respectively. The calculated flux densities of the vertical radio structure are 5.0 ± 0.9 mJy at 235 MHz and 3.8 ± 0.5 mJy at 610 MHz. The integrated spectral index is ∼−0.3, which indicates a flat spectrum for this structure and is significantly

Downloaded from https://academic.oup.com/mnras/article/470/3/3742/3867312 by CNRS - ISTO user on 08 August 2022

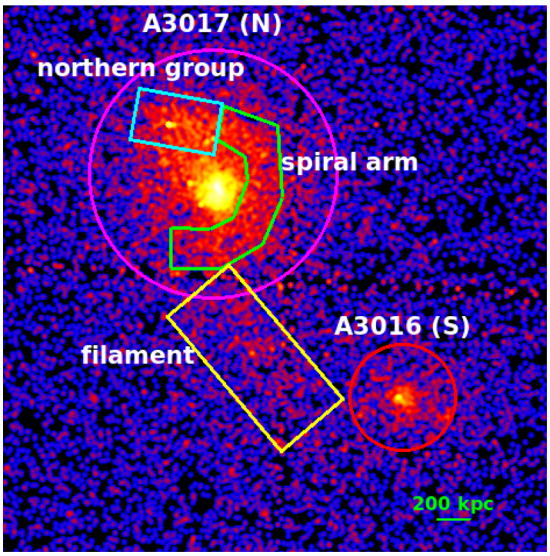


Figure 3. A3017 X-ray image showing the different regions from which X-ray spectra were extracted.

flat if this is a typical extended radio galaxy. We confirmed that there is no corresponding optical counterpart within 30 arcsec of the strongest northern peak (Fig. 2c). Furthermore, at this position there is no radio source identified in the 843 MHz SUMSS catalogue or 150 MHz TGSS.

2.4 X-ray spectral analysis

We extract the spectra from the A3017, filament, northern infalling group, spiral arm and south X-ray cluster regions after subtracting the background (Fig. 3). Since we do not have enough counts in our data, estimating the temperatures of the cavities is very difficult and leads to high uncertainties. However, we estimated the significance for the detection of the filament around A3017. We calculated that the total counts within the filament region (see below) are ∼1750 and the average background counts are ∼1050, leading to an S/N of ∼16. We apply an apec model with photoelectric absorption (wabs) for which we have fixed the hydrogen column density to 0.02×10^{22} atoms cm^{-2}, the metal abundance to 0.3 solar, also reduced to 0.2 and 0.1 for the filament, and the redshift to 0.2195. In this analysis, we used the solar abundance table in the CIAO SHERPA spectral fitting package from Asplund et al. (2009). We grouped spectral data so that each bin has at least 20 counts. In our spectral fitting we considered the energy range between 0.5 and 2.5 keV. We simultaneously fit the spectra from both *Chandra* observations (Table 2).

To extract the spectra from the filament, we used a box of size ($l \times b$) 135 arcsec × 300 arcsec (480 × 1065 kpc^2, $r = 68$ arcsec). We found a temperature of $3.4^{-0.8}_{+1.3}$ for $Z = 0.3$ solar. The corresponding density is $7.7^{-0.24}_{+0.27} \times 10^{-4}$ cm^{-3}. Since we do not know the abundance fraction in the low-density filament region, we tried two other values. For $Z = 0.2$ solar, the temperature is $3.1^{-0.71}_{+1.14}$ and the density is $7.8^{-0.29}_{+0.32} \times 10^{-4}$ cm^{-3}. For $Z = 0.1$ solar, the temperature is $2.8^{-0.63}_{+1.12}$ and the density is $8.1^{-0.38}_{+0.43} \times 10^{-4}$ cm^{-3}. We used circular regions of radii 3.5 arcmin and 1.5 arcmin for the A3017 (north) and south X-ray clusters, respectively, to extract the spectra. For the northern group, we took a 86 arcsec × 142 arcsec box region and for the spiral arm a 360° polygon region around the arm region, as shown in Fig. 3. We have listed the temperature, normalization and flux density values for the five regions in Table 4 with 1σ uncertainties.

3 OPTICAL ANALYSIS

This section investigates the optical properties of the galaxy cluster A3017 as well as the filament structure attached to it. This has been done by using available catalogues extracted from the WISE and European Southern Observatory (ESO) Red public surveys.

Galaxy clusters are well characterized by old- and early-type members that correspond to red galaxies. Multiband optical data has been used to obtain the colour magnitude diagram (CMD; Fig. 4). For this, the WISE and SuperCOSMOS catalogues (ESO Red survey) were cross matched (tolerance radius = 6 arcsec). The R-3.4μm colour was plotted against the R magnitude. Only galaxies (corresponding to Class = 1 in SuperCOSMOS catalogue) have been considered. Further, within the Class 1 sources, galaxies within the magnitude range $R = 17$–21.5 were chosen; these are approximately the limits for the BCG magnitude and for the ESO RED-R survey magnitude limit. The most likely red sequence region in the CMD is in the range of colours 3–3.5. The linear regression fit was applied to galaxies only within this magnitude range. A slightly negative slope ($m = -0.0574$) is found, indicating the variation of metallicity across the galaxies with magnitude. We identify groups of galaxies in the northern area of the A3017 cluster (black dashed circles) as well as the filament protruding from it. The majority of the galaxies in the cluster and above-mentioned regions fall within the selected colour range.

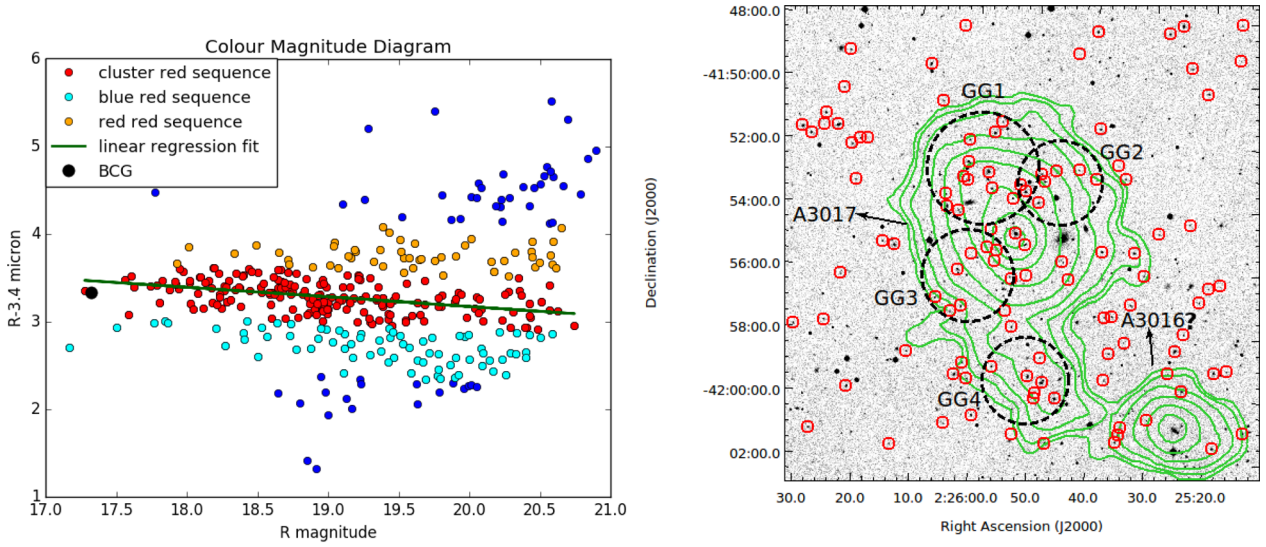
4 DO A3017 AND A3016 FORM A PAIR OF CLUSTERS?

In order to see how the galaxies are distributed in the field, we built a density map based on the red sequence galaxies of A3017. The density map was computed with an adaptive kernel as explained in Durret et al. (2016), with a pixel size of 18 arcsec and 100 bootstraps, and the significance contours were computed as explained in that paper. The corresponding density map is shown in Fig. 5 (left). We

Table 4. A3017 *Chandra* spectral analysis. These values are measured in soft energy (0.5–2.5 keV) band.

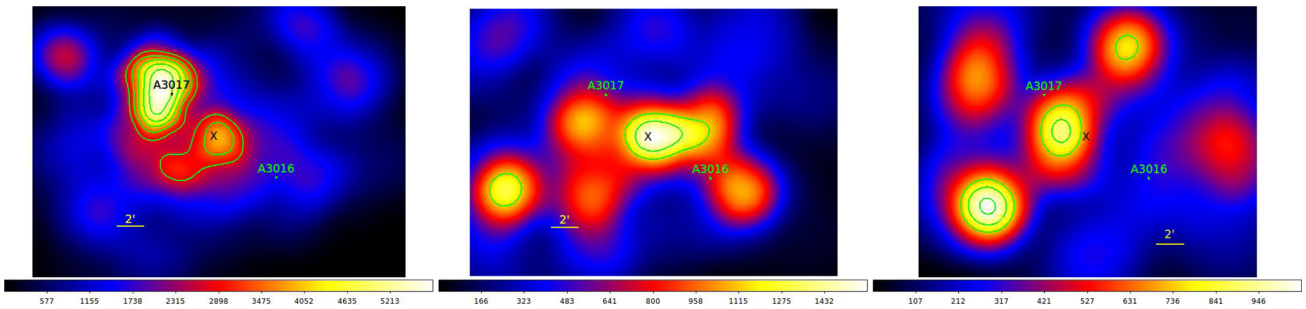
Cluster region	Counts	χ^2/degree of freedom	Temp. (keV)	Normalization (10^{-4})	Flux (10^{-13} cgs)
A3017	5611	171/241	$5.8^{-0.6}_{+0.6}$	$56^{-0.7}_{+0.7}$	32
Filament	427	36/47	$3.4^{-0.8}_{+1.3}$	$3.8^{-0.2}_{+0.3}$	2.1
South X-ray cluster	574	40/54	$3.7^{-0.7}_{+1.2}$	$5.1^{-0.3}_{+0.3}$	2.8
Spiral arm	1000	101/178	$6.0^{-0.8}_{+0.9}$	$7.1^{-0.3}_{+0.3}$	6.9
Northern group	566	90/104	$3.8^{-0.7}_{+1.4}$	$6.4^{-0.3}_{+0.3}$	3.6

Downloaded from https://academic.oup.com/mnras/article/470/3/3742/3867312 by CNRS - ISTO user on 08 August 2022



(a) (b)

Figure 4. Left: R-3.4 μm colour against *R* magnitude for the galaxies in the A3017 area, taken from the SuperCOSMOS and ESO Red catalogues. The red filled circles show the galaxies belonging to the cluster red sequence, indicated by the green line, the yellow filled circles correspond to the 'red red sequence' and the cyan filled circles correspond to the 'blue red sequence' (see the text). Right: SuperCOSMOS optical image of A3017. Green contours show the X-ray emission and red circles show the member galaxies. Black dashed circles indicate possible groups of galaxies at the redshift of A3017.



(a) (b) (c)

Figure 5. Left: density map for the galaxies located along the red sequence of A3017 (the red points in Fig. 4a). Middle: density map for the galaxies located below the red sequence of A3017. Right: density map for the galaxies located above the red sequence of A3017. The significance contours start at 3σ and increase by steps of 1σ. The positions of A3017 and A3016 are shown with tiny circles. The position of G256.55–65.69 (see text) is indicated with an X. North is top and east is left.

see that A3017 is detected at a 7σ level. A second structure halfway between A3017 and A3016 is also detected at a 4σ level, while we see absolutely no signal at the position of A3016 [at the position given by NASA/IPAC Extragalactic Database (NED)].

This very puzzling result led us to question the redshift of A3016. First, we can note that Simbad gives a redshift $z = 0.2195$ for this cluster (Planck Collaboration VIII 2011) while NED gives no redshift for this cluster. Secondly, there are extremely few references on A3016 in the literature.

So, we decided to extract from our catalogue the galaxies along a 'blue red sequence' and a 'red red sequence', with the same slope and width of ±0.3 as the A3017 RS, but located at colours 0.6 mag below and above the RS, respectively. The corresponding density maps are shown in Fig. 5 (middle and right). We can see that A3016 is detected in neither of them. The image built with galaxies bluer than A3017 shows a quite intense structure between A3017 and A3016. Less than 0.5 arcmin from the peak of this structure is located a galaxy cluster (hereafter cluster X) named [BM78] 231 in NED (at coordinates RA: $02^{h}25^{m}40\overset{s}{.}1$, Dec.: $-41^{\circ}57'31''$, no redshift available). The position of this cluster is marked with an X on the figure. The image built with galaxies redder than A3017 shows two intense structures, one about 1.8 arcmin east of cluster X and one further to the southeast. We could not identify either of these structures with a galaxy cluster in NED.

The two possible explanations to the fact that A3016 is not detected in these density maps are as follows: (1) it is not a cluster and the X-ray detection as an extended source is wrong (which is rather surprising in view of the good spatial resolution of *Chandra*); (2) it is too distant to be detected in our rather shallow optical data. In any case, the hypothesis that we are observing a pair of clusters is most probably not correct, and A3017 does not form a pair with A3016.

5 DISCUSSION AND CONCLUSION

There is a hot X-ray filament associated with A3017 cluster implying a significant baryon overdensity in the filament region. This overdense filament appears to be connected with another X-ray cluster. We estimate temperatures of $\sim 5.8^{-0.57}_{+0.62}$ keV for A3017 and

Downloaded from https://academic.oup.com/mnras/article/470/3/3742/3867312 by CNRS - ISTO user on 08 August 2022

$3.7^{-0.73}_{+1.22}$ keV for the south X-ray cluster. The temperature of group-sized systems is usually $\lesssim$1 keV (Bahcall 1996; Rosati, Borgani & Norman 2002), hence this X-ray emission is most probably related to the cluster ICM than to a group. Current multiwavelength observations show that cluster mergers have several stages (Parekh et al. 2015, and references therein): beginning with the early stage when two bodies are approaching each other, followed by first interaction, mixing of the hot gases, violent collision and shock production, turbulence injection, ram pressure stripping, the intermediate stage when the two bodies are receding from each other and finally the merger and relaxation on a time-scale of a few gigayears. From the optical data for A3017, it becomes clear that A3017 is an early stage merger because the positions of the brightest central galaxies are still associated with the X-ray peaks. In a late stage merger, the galaxies and ICM are often distributed differently. There could be a weak shock present in the A3017 filament as in the cases of A222/A223 and CIZA J1358.9-4750. The presence of a weak shock in the filament could be responsible for the linear vertical radio structure visible in the radio map (Fig. 2). However, present X-ray data are not sufficient to estimate the properties of the shock in the filament. In simulations, Akahori & Yoshikawa (2010) have shown that in the early stage of a merger ($t \approx 0.5$ Gyr), two clusters interact with each other at the outskirts and then create linked regions (filaments or bridges) where the ICM is compressed due to the collision. Further, these authors have postulated that there exist shock fronts with Mach numbers $M \sim$ 1.5–2.0 at the positions of the bridge regions. These shocks are immediately formed at the contact interface of the two clusters when the clusters begin to collide, and they then propagate in a direction perpendicular to the merger axis outside of each cluster, forming outgoing merger shocks (Bagchi et al. 2006). However, in the present case, there is no strong evidence that the south X-ray cluster is at the same redshift as A3017, based on the galaxy density map analysis, so these two clusters do not form a binary cluster merger. We need further optical spectroscopic information to prove or disprove whether the X-ray bridge is connecting two binary clusters or is only associated with A3017 as a hot X-ray tail (De Filippis et al. 2004; Sun et al. 2006; Schellenberger & Reiprich 2015).

We estimate temperatures of $3.4^{-0.77}_{+1.30}$ for the A3017 filament, assuming $Z = 0.3$ solar. The temperature of the filament is hotter than expected, so the hot gas in the filament is probably the ICM from the cluster outskirts, with some contamination by cluster gas also. We calculated that the density of the filament is between $\sim 7.5 \times 10^{-4}$ and $\sim 8.1 \times 10^{-4}$ cm^{-3}, its mass $\sim$4.2–4.5 $\times 10^{12}$ M$_\odot$ and its entropy $\sim$320–405 keV cm^2, for metallicities between $Z_\odot = 0.3$ and 0.1. To calculate these values, we assumed the volume of the filament to be a cylinder of size 135 arcsec $\times$ 300 arcsec (480 kpc $\times$ 1065 kpc). Accretion shocks heat the cluster outskirts ($>R_{200}$) (Molnar et al. 2009) raising entropies above 1000 keV cm^2. This entropy is expected to increase further out to the virial radius. In this case, the low entropy of the filament suggests that the radiating hot gas in the A3017 filament has not yet been reached by the shock-heating operating on the ICM in the cluster outskirts.

The core region of A3017 is cool, with an estimated central cooling time of $\sim$1.4 Gyr,[1] and no sign of disturbances in the X-ray surface brightness distribution. There are substructures, two opposite cavities and a spiral arm visible in the core region and surrounding it. The cavities are filled with radio emission at 235 and 610 MHz, and they are very likely large empty bubbles evacuated by the AGN's radio lobes. Current low-resolution radio data are not sufficient to resolve the jet emission from the AGN. A spiral feature is also visible which is in good agreement with gas sloshing in connection with a subcluster or group merger. There is also an excess of X-ray emission visible in the north-east direction which is associated with subgroup GG1 as marked in Fig. 4. We estimated the temperature of this group to be $3.8^{-0.7}_{+1.4}$ keV, which is more typical of a small cluster. This small cluster could be infalling on to the main cluster body of A3017. The entropy of this infalling group is $\sim$220 keV cm^2. There is another subgroup GG2 also associated with the large spiral arm. Generally, steep spectrum mini-radio haloes of the size $\sim$100–500 kpc are expected in cool core clusters and believed to be directly connected with turbulent re-acceleration in gas sloshing activity (ZuHone, Markevitch & Brunetti 2011). However, we have not detected any diffuse radio emission in the present radio data.

The radio detection of filaments can probe the distribution of cosmic rays and magnetic fields in the cosmic web (Vernstrom et al. 2017), but such a detection is very challenging, due to the extremely low magnetic field (10–100 nG) and to the inefficiency of relativistic particle acceleration (Vazza et al. 2015). However, simulations (Araya-Melo et al. 2012; Vazza et al. 2015) predict that it is possible to detect filaments in radio observations if the shocks accelerate the electrons sufficiently. In current observations, there is no detection of radio emission in the filament region of A3017. Hence, we calculate the upper limit on the radio luminosity of the filament. We calculated this upper limit (with the 610 MHz radio data) by first measuring the rms in the X-ray filament assuming the same cylindrical region as mentioned above. This rms is measured for a single beam, so we need to scale it with a factor of $\sqrt{(\text{size}^2/\text{beam˜area})}$ to take into account the number of beams within the total filament size. Assuming the 135 arcsec $\times$ 300 arcsec filament size from the X-ray measurement, we found an upper limit to the radio power of the filament of $<$23.95 W Hz^{-1} at 610 MHz at the 3σ level. It will be important to observe such overdense and hot X-ray filaments around clusters and between cluster pairs with future high-sensitive radio telescopes such as SKA, MeerKAT and ASKAP to constrain the magnetic field in filaments.

ACKNOWLEDGEMENTS

We thank the referee for some useful comments. MBP gratefully acknowledges the support of Department of Science and Technology (DST), New Delhi, under the INSPIRE faculty Scheme (sanctioned no. DST/INSPIRE/04/2015/000108). This research has made use of the data from *Chandra* archive and of software provided by the Chandra X-ray Centre (CXC) in the application packages CIAO, CHIPS and SHERPA. This research has also made use of NASA's Astrophysics Data System of the NASA/IPAC Extragalactic Database (NED) which is operated by the Jet Propulsion Laboratory, California Institute of Technology, under contract with the National Aeronautics and Space Administration and of the SIMBAD data base, operated at CDS, Strasbourg, France. Facilities: *Chandra* (ACIS), *HST* (ACS). We thank the staff of the GMRT who have made these observations possible. GMRT is run by the National Centre for Radio Astrophysics of the Tata Institute of Fundamental Research. We also thank Huib Intema for providing SPAM package for reducing GMRT data.

[1] $t_{\rm cool} = 69 \left(\frac{n_e}{10^{-3}\ {\rm cm}^{-3}}\right)^{-1} \left(\frac{T}{10^8\ {\rm K}}\right)^{1/2}$ Gyr.

Downloaded from https://academic.oup.com/mnras/article/470/3/3742/3867312 by CNRS - ISTO user on 08 August 2022

REFERENCES

Akahori T., Yoshikawa K., 2010, PASJ, 62, 335
Araya-Melo P. A., Aragón-Calvo M. A., Brüggen M., Hoeft M., 2012, MNRAS, 423, 2325
Ascasibar Y., Markevitch M., 2006, ApJ, 650, 102
Asplund M., Grevesse N., Sauval A. J., Scott P., 2009, ARA&A, 47, 481
Bagchi J., Durret F., Neto G. B. L., Paul S., 2006, Science, 314, 791
Bahcall N. A., 1996, preprint (astro-ph/9611148)
Blanton E. L., Randall S. W., Clarke T. E., Sarazin C. L., McNamara B. R., Douglass E. M., McDonald M., 2011, ApJ, 737, 99
Buote D. A., Zappacosta L., Fang T., Humphrey P. J., Gastaldello F., Tagliaferri G., 2009, ApJ, 695, 1351
De Filippis E., Bautz M. W., Sereno M., Garmire G. P., 2004, ApJ, 611, 164
Dietrich J. P., Werner N., Clowe D., Finoguenov A., Kitching T., Miller L., Simionescu A., 2012, Nature, 487, 202
Dolag K., Bykov A. M., Diaferio A., 2008, Space Sci. Rev., 134, 311
Durret F., Lima Neto G. B., Forman W., Churazov E., 2003, A&A, 403, L29
Durret F., Lima Neto G. B., Forman W., 2005, A&A, 432, 809
Durret F. et al., 2016, A&A, 588, A69
Eckert D. et al., 2015, Nature, 528, 105
Intema H. T., 2014, in Chengalur J. N., Gupta Y., eds, ASI Conf. Ser. Vol. 13, SPAM: A data reduction recipe for high-resolution, low-frequency radio-interferometric observations. p. 469
Intema H. T., van der Tol S., Cotton W. D., Cohen A. S., van Bemmel I. M., Röttgering H. J. A., 2009, A&A, 501, 1185
Intema H. T., Jagannathan P., Mooley K. P., Frail D. A., 2017, A&A, 598, A78
Kull A., Böhringer H., 1999, A&A, 341, 23
Markevitch M., Vikhlinin A., 2007, Phys. Rep., 443, 1
McNamara B. R., Nulsen P. E. J., 2007, ARA&A, 45, 117
McNamara B. R., Nulsen P. E. J., 2012, New J. Phys., 14, 055023
Molnar S. M., Hearn N., Haiman Z., Bryan G., Evrard A. E., Lake G., 2009, ApJ, 696, 1640
Parekh V., van der Heyden K., Ferrari C., Angus G., Holwerda B., 2015, A&A, 575, A127
Paterno-Mahler R., Blanton E. L., Randall S. W., Clarke T. E., 2013, ApJ, 773, 114
Planck Collaboration VIII, 2011, A&A, 536, A8
Planck Collaboration VIII, 2013, A&A, 550, A134
Rosati P., Borgani S., Norman C., 2002, ARA&A, 40, 539
Scaife A. M. M., Heald G. H., 2012, MNRAS, 423, L30
Schellenberger G., Reiprich T. H., 2015, A&A, 583, L2
Springel V. et al., 2005, Nature, 435, 629
Sun M., Jones C., Forman W., Nulsen P. E. J., Donahue M., Voit G. M., 2006, ApJ, 637, L81
Vazza F., Ferrari C., Brüggen M., Bonafede A., Gheller C., Wang P., 2015, A&A, 580, A119
Vazza F., Ferrari C., Bonafede A., Brüggen M., Gheller C., Braun R., Brown S., 2015, Proc. Sci., Filaments of the Radio Cosmic Web: opportunities and challenges for SKA. SISSA, Trieste, PoS#97
Vernstrom T., Gaensler B. M., Brown S., Lenc E., Norris R. P., 2017, MNRAS, 467, 4914
Vikhlinin A. A., Markevitch M. L., 2002, Astron. Lett., 28, 495
Werner N., Finoguenov A., Kaastra J. S., Simionescu A., Dietrich J. P., Vink J., Böhringer H., 2008, A&A, 482, L29
ZuHone J., Markevitch M., Brunetti G., 2011, Mem. Soc. Astron. Ital., 82, 632
ZuHone J. A., Markevitch M., Lee D., 2011, ApJ, 743, 16

This paper has been typeset from a TEX/LATEX file prepared by the author.

Downloaded from https://academic.oup.com/mnras/article/470/3/3742/3867312 by CNRS - ISTO user on 08 August 2022